Article

Miniaturized Metalens Based Optical Tweezers on Liquid Crystal Droplets for Lab-on-a-Chip Optical Motors

Satayu Suwannasopon [1,2,3], **Fabian Meyer** [3], **Christian Schlickriede** [3], **Papichaya Chaisakul** [1], **Jiraroj T-Thienprasert** [1], **Jumras Limtrakul** [2,4], **Thomas Zentgraf** [3] **and Nattaporn Chattham** [1,2,*]

[1] Department of Physics, Faculty of Science, Kasetsart University, Bangkok 10900, Thailand; satayu.suw@ku.th (S.S.); fscipac@ku.ac.th (P.C.); chorawut@ku.ac.th (J.T.-T.)

[2] Center for Advanced Studies in Nanotechnology for Chemical, Food and Agricultural Industries, KU Institute for Advanced Studies, Kasetsart University, Bangkok 10900, Thailand

[3] Department of Physics, Paderborn University, D-33098 Paderborn, Germany; fabian.meyer@uni-paderborn.de (F.M.); christian.schlickriede@uni-paderborn.de (C.S.); thomas.zentgraf@uni-paderborn.de (T.Z.)

[4] Vidyasirimedhi Institute of Science and Technology, Rayong 21210, Thailand; jumras.limtrakul@vistec.ac.th

[*] Correspondence: nattaporn.c@ku.ac.th

Abstract: Surfaces covered with layers of ultrathin nanoantenna structures—so called metasurfaces have recently been proven capable of completely controlling phase of light. Metalenses have emerged from the advance in the development of metasurfaces providing a new basis for recasting traditional lenses into thin, planar optical components capable of focusing light. The lens made of arrays of plasmonic gold nanorods were fabricated on a glass substrate by using electron beam lithography. A 1064 nm laser was used to create a high intensity circularly polarized light focal spot through metalens of focal length 800 μm, N.A. = 0.6 fabricated based on Pancharatnam-Berry phase principle. We demonstrated that optical rotation of birefringent nematic liquid crystal droplets trapped in the laser beam was possible through this metalens. The rotation of birefringent droplets convinced that the optical trap possesses strong enough angular momentum of light from radiation of each nanostructure acting like a local half waveplate and introducing an orientation-dependent phase to light. Here, we show the success in creating a miniaturized and robust metalens based optical tweezers system capable of rotating liquid crystals droplets to imitate an optical motor for future lab-on-a-chip applications.

Keywords: metalens; metamaterials; Pancharatnam-Berry phase; optical tweezers; optical trap; liquid crystal droplets

1. Introduction

Metamaterials are artificial materials with unusual properties that have emerged from a structural arrangement rather than composition. By directly designing the arrangement of meta-atoms, extraordinary properties of light propagation beyond nature availability can be achieved [1–3]. For over twenty years, this emerging field of metamaterials has capture enormous interest from scientists to explore unique optical effects such as cloaking, negative refraction or ultrathin lenses. Powerful and sophisticate electromagnetic modeling software, nowadays, is able to accurately simulate and predict the response of pattern design before fabrication attempt. The success in creating metamaterials in the visible light region was first reported in 2007 [4]. A novel type of metamaterial consisting of planar arrays of artificial nanostructures on ultrathin layers—so-called metasurfaces—capable of light

manipulation have recently been discovered [5–8]. Most metasurfaces studied so far typically comprise of plasmonic nanoantennas of designed shape and orientation pattern on thin substrates. The optical property difference between the antennas and surrounding medium results in optical interaction generating and controlling the dispersion of light, amplitude, phase profile and polarization response along the interface [9]. Recently, several potential applications of metasurfaces have been suggested, which have been led to the development of ultrathin devices such as waveplates for generating vortex beam, beam steering, holography, aberration-free quarter waveplates (QWPs), spin-hall effect of light and spin-controlled photonics, unidirectional surface plasmon polariton excitation and ultrathin metalenses [6,7,10–16].

Metalenses have emerged from the advance in the development of metasurfaces providing a new basis for recasting traditional lenses into thin, planar optical components, having similar or even better performance at smaller scales. In the near future with higher efficiency and cheaper production, these metalenses have a high potential to replace traditional lenses in several applications, e.g., imaging systems, optical data storage, laser printing, and optical communications [17]. Their ultrathin sizes can also benefit the development of optical Lab-on-a-chip (LOC) devices. The aim of this work is to evaluate the potential of plasmonic metasurfaces acting as a phase mask on a substrate material to modify the beam shape of laser light for polarized optical trapping, following the recent success on the first planar metalens optical trap in microfluidic system [18–20]. For most laboratories, drawbacks of optical trapping have been the high cost involving large equipment like a microscope as well as the difficulty to build and maintain such systems. To overcome these inconveniences, we applied metalenses to create a circularly polarized optical tweezer system as a handheld device and test it on a particle trap and localization of birefringent liquid crystal droplets.
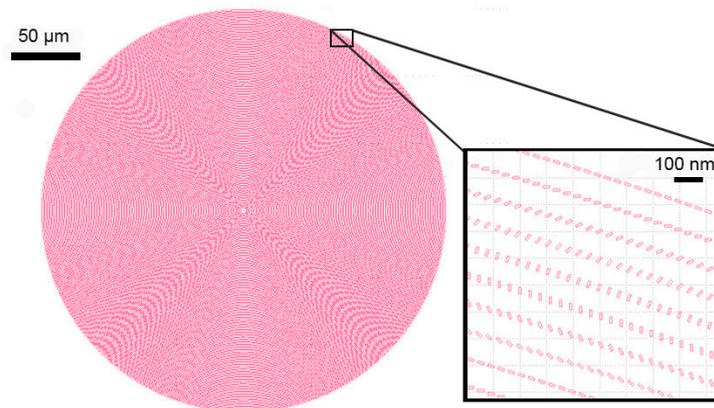
2. Materials and Methods

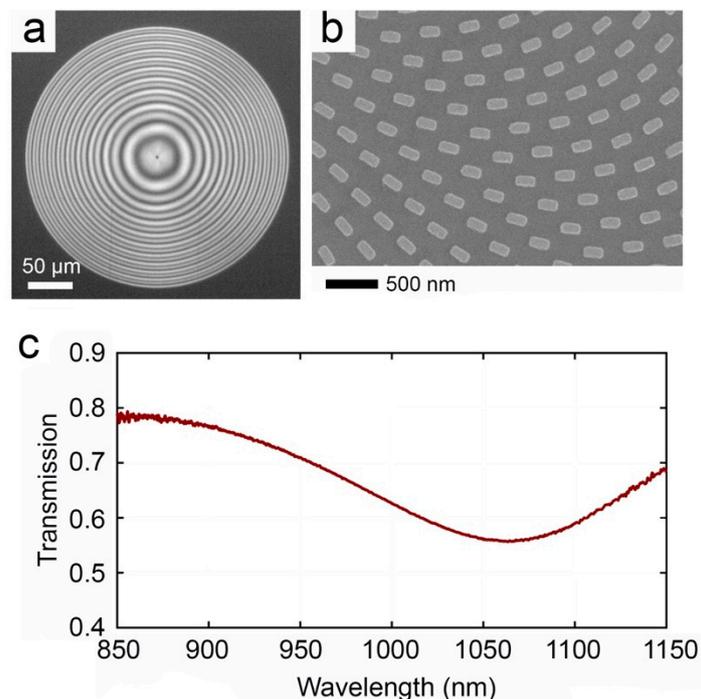### 2.1. Design and Fabrication of the Metalens

We evaluate the potential of a plasmonic metalens to tightly focus the beam shape of laser light for optical trapping and particle manipulation. Laser light that passes through the metasurface experiences arbitrary continuous phase gradients that can be spatially tailored by utilizing the accumulated Pancharatnam-Berry phase during a polarization conversion for circularly polarized light [21]. For this concept, each nanostructure acts like a local half waveplate, which introduces an orientation-dependent phase to the light. In order to fabricate the structures of the plasmonic metasurfaces, we performed design operation with MATLAB FDTD and CST Microwave Studio. Based on the concept of interfacial phase discontinuities [8], these software were used for configuring lens pattern and simulation of the scattering response of plasmonic nanoantennas. Simulation results for a metalens' pattern of 800 μm focal length are shown in Figure 1. Arrays of plasmonic nanorods made of gold were fabricated on a glass substrate by using electron beam lithography (EBL). For the fabrication process, a thin layer of indium tin oxide (ITO) was used on top of the substrate to obtain conductivity for the EBL. After writing the structure with EBL, the electron beam resist was used as a mask for subsequent thermal evaporation of a 40 nm thick gold layer and which was later removed by a lift-off process. Based on this process, a metalens for 1064 nm left circularly polarized light incident beam was obtained with diameter 300 μm and focal length of f = 800 μm with N.A. = 0.6, as shown in a photomicrograph in Figure 2a. A scanning electron microscopy (SEM) image of the lens (Figure 2b) illustrates each nanorod of dimension $90 \times 220 \times 40 \, \text{nm}^3$ placed with a defined orientation angle φ serving as meta-atom. In order to function as a conventional spherical lens, the phase profile $\varphi(x, y)$ of the metalens is calculated by the following equation [16]:

$$\varphi(x, y) = \frac{2\pi}{\lambda} \left(\sqrt{x^2 + y^2 + f^2} - f \right) \tag{1}$$

where f is the focal length of the lens, λ is wavelength in free space, x and y are coordinates of each nanorod. The Pancharatnam-Berry phase is usually perceived by plasmonic rectangular nanorod. When circularly polarized light of handedness σ is incident upon a nanorod with in-plane orientation angle θ, light transmitted through this nanorod would be distinguished into two parts: one with the same handedness with no phase delay and the other with a phase delay of $\varphi = 2\sigma\theta$. By placing nanorods with orientation θ as designed, one can control phase of light at a certain wavelength through metalens [22,23]. The period is chosen such that lattice resonances by the periodic arrangement are at different wavelengths.

Figure 1. Simulated pattern of 800 μm focal length metalens with a closer view of nanoantenna alignment at the edge of the lens.

Figure 2. The schematic of plasmonic metalens designed for the focal length of 800 μm. (**a**) Optical microscopy image of the metalens surface. The scale bar is 50 μm, (**b**) SEM image of part of the lens showing the gold nanorods. The scale bar is 500 nm. (**c**) Measurement of the FTIR transmission spectra of the metalens showing localized surface plasmon polariton resonance at 1064 nm.

The lens was tested with Fourier Transform Infrared Spectroscopy (FTIR, Bruker, Ettlingen, Germany) showing localized surface plasmon polariton resonance in the transmission spectra at 1064 nm (Figure 2c) according to the design. The dip in the transmission is caused by the excitation of

the localized surface plasmon polariton modes in the metal nanostructures. This mode interacts with the incident light and leads to scattering and absorption. Hence, the transmission at target wavelength is lower than that for other wavelengths.

2.2. Optical Trapping of Particles with the Metalens

Optical tweezers are normally formed by tightly focused laser beams with a high numerical aperture objective lens. It has been widely used for manipulation of small particles without direct mechanical interaction with the surrounding. The laser beam can trap particles based on two types of forces, namely, scattering and gradient forces. Scattering force causes from momentum transfer of scattered photons to a particle pushing the particle in the propagation direction of the incident light. This force is proportional to intensity of light and tends to destabilize the trap, however, with tightly focused laser beam, the gradient force acts to draw the particle towards the beam focus. The scattering force, $\vec{F}_s$, can be explained by the following equation [24]:

$$\vec{F}_s = n_m \frac{\sigma \langle \vec{S} \rangle}{c} = n_m \frac{\sigma I \langle \vec{r} \rangle}{c} \hat{z} \tag{2}$$
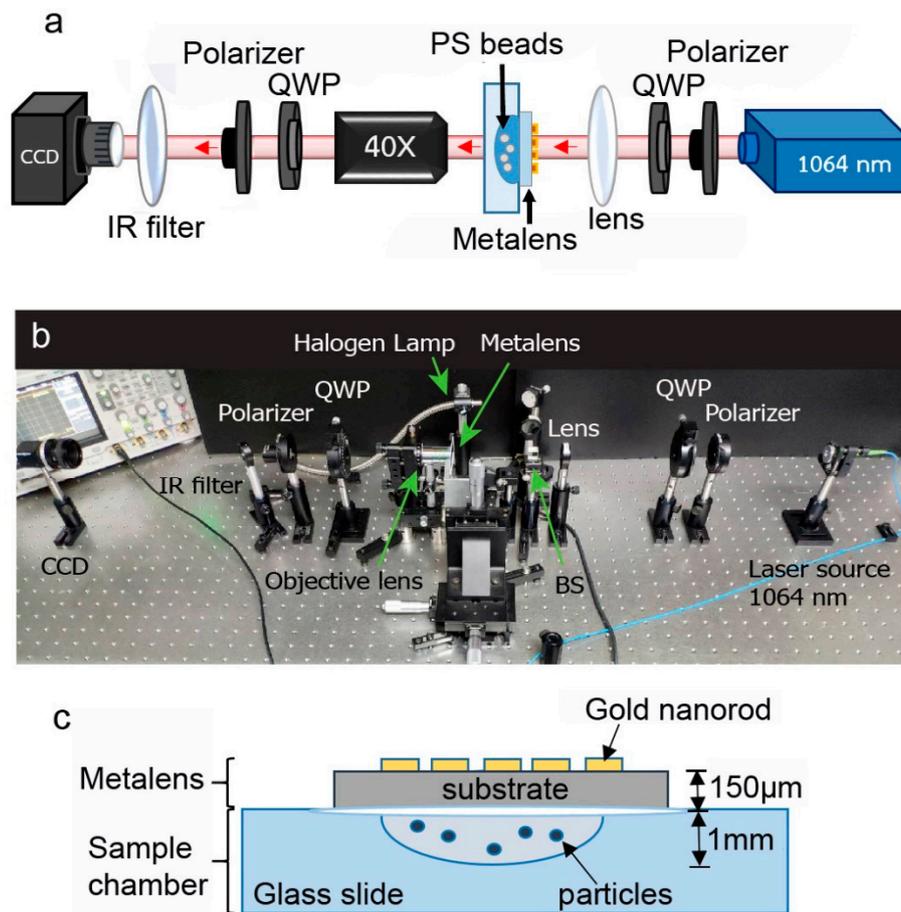
where $\langle \vec{S} \rangle$ is the time-averaged Poynting vector which is equal to the intensity of incident beam, σ is the scattering cross-section of trapped object depending on the ratio of refractive index (n_p/n_m); n_p, n_m is the refractive index of particle and medium respectively and c is the speed of light in the vacuum.

The gradient force, $\vec{F}_{grad}$, arises from the law of conservation of momentum by the interaction of photon pressure of the incident laser beam against the surface of the trapped particle. Stable trapping causes from the gradient force by diverging the beam away from the focal point. Then the particle will experience the restoring force pulling it back toward the beam axis. This gradient force, which acts like restoring force is proportional to the gradient of the light intensity explained by the following equation:

$$\vec{F}_{grad}(\vec{r}) = \frac{1}{2n_m \varepsilon_0 c} \alpha \vec{\nabla} I(\vec{r}) \tag{3}$$

where $I(\vec{r})$ is intensity, ε is dielectric constant in vacuum and α is the polarizability which depends on the refractive index ratio (n_p/n_m).

The experimental setup used for optical trapping of a polystyrene bead (Polysciences, Inc.) with the metalens is shown in Figure 3a,b. A CW 1064 nm fiber laser operated at 300 mW is used as a laser source. The incident beam was made circularly polarized by a Glan-Thompson polarizer and a quarter waveplate. The sample chamber is made from a glass slide chamber filled with 4.5 μm polystyrene beads in water and glued on top with metalens (Figure 3c). A convex lens is inserted in between a quarter waveplate and the sample to ensure that laser beam covers all surface area of metalens for high efficiency of nanoantenna radiation. The movement of the beads is observed by a CCD camera with a 40X objective lens. A light Illumination path is composed of a halogen fiber optic light source, a mirror, a lens and a beamsplitter (BS) as shown in Figure 3b. Light beam passed through the sample by placing a beamsplitter in front of the metalens chamber for illumination. The output laser was tested to be circularly polarized by inserting another set of a quarter waveplate and a linear polarizer. To find the trapping strength of the optical tweezers, the trapping laser was modulated by frequency modulator in the range of 1 to 10 kHz with a step size of 0.5 kHz [25]. A tracker software was used to track the beads and locate their position in the laser trap at different modulation frequencies.
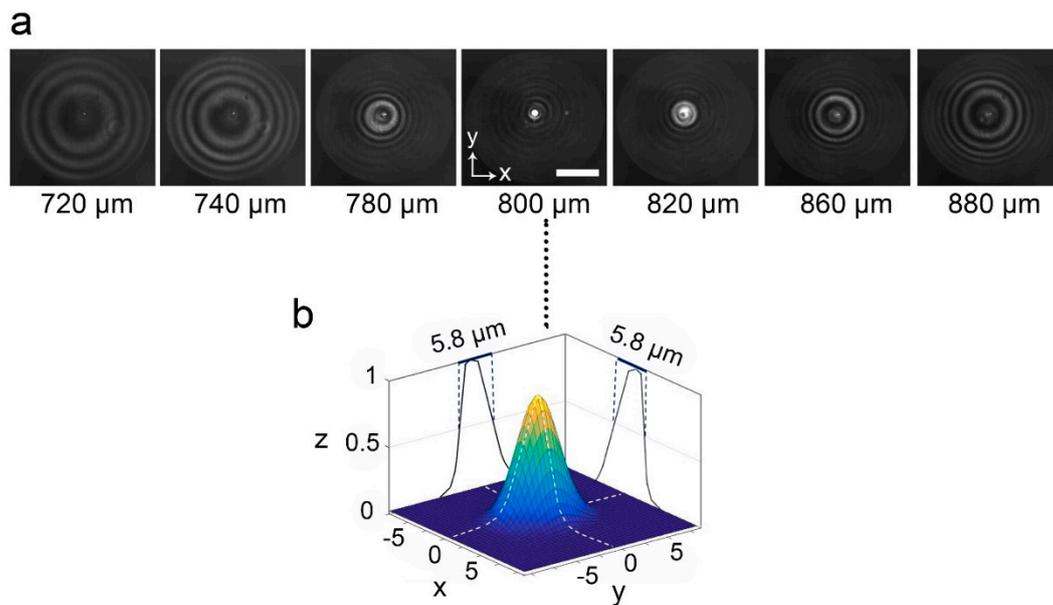
Figure 3. (**a**) An experimental setup diagram of metalens based on optical tweezers with (**b**) a laboratory setup illustrated. Note that a straight beam path from the laser to a CCD camera is for optical trapping and an illumination path with a halogen lamp as a light source is set on the side to enter the optical trapping path through a beamsplitter (BS). (**c**) Schematic sketch of the chambered glass slide, which was attached on top with metalens as a sample container.
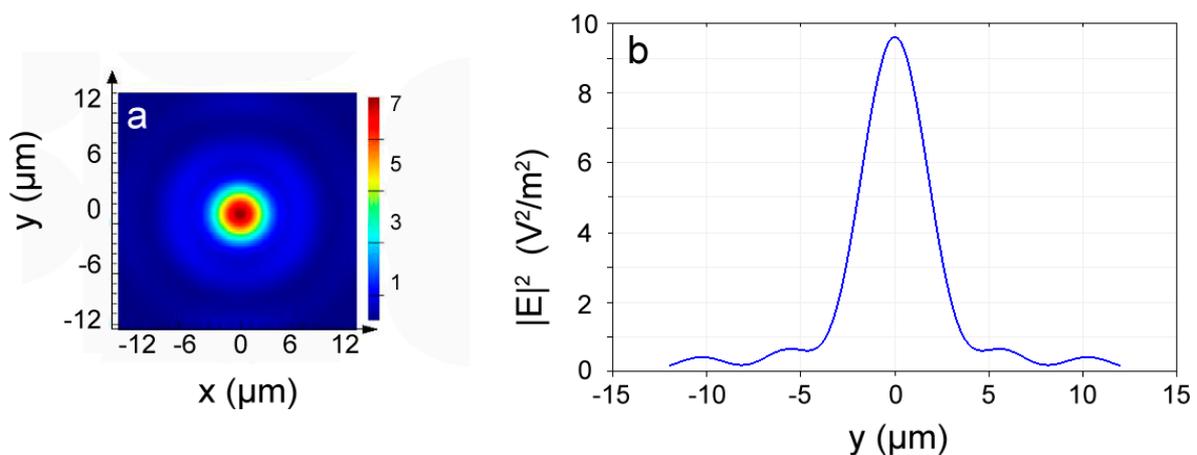
A circularly polarized laser trap can perform its great advantage on rotating birefringence object by conservation of angular momentum law [26]. The setup was tested with birefringent nematic liquid crystal (NLC) droplets filled inside the metalens chamber. The droplets were prepared by dispersion of 5CB (4-cyano-4'-pentylbiphenyl, SIGMA-ALDRICH) in water with CTAB (Hexadecyltrimethyl ammonium bromide) as a surfactant. By controlling the CTAB concentration, either bipolar or radial NLC droplet or both configurations can be achieved [27,28].
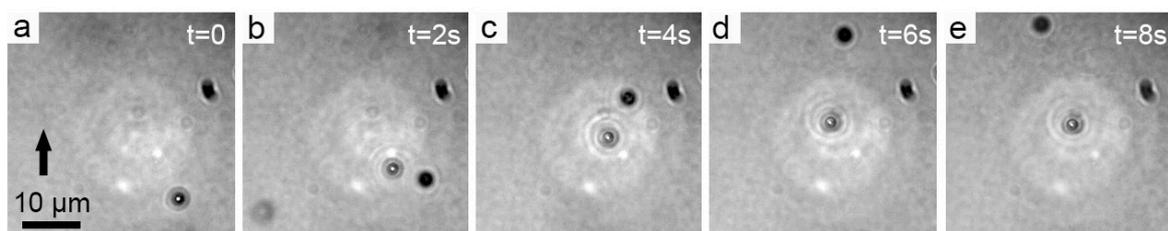
3. Results and Discussion

The interaction of the left circularly polarized laser beam with 30 mW power passing through the metalens resulted in the intensity profile of the focal spot at different locations from the lens as shown in Figure 4a. The laser spot was focused sharply at 800 ± 2 µm corresponding to the lens design. Interpolation of the intensity measurement at the focal length is depicted in Figure 4b with a full width at half maximum (FWHM) of 5.8 ± 0.1 µm. The focal spot intensity obtained by a Lumerical FDTD simulation is illustrated in Figure 5 showing the beam profile with FWHM closely similar to one obtained from experimental observation of Figure 4. The optical trapping experiment was then performed with 4.5 µm polystyrene beads in water that were introduced into the sample chamber shown in Figure 3. The trapping experiments were successfully conducted with 30 mW laser power as shown in Figure 6.

Figure 4. (**a**) The measurement of the intensity distribution at different locations from the metalens surface for 1064 nm laser light with 30 mW power. The scale bar is 50 μm. The laser beam was focused sharply at 800 μm corresponding to the design. (**b**) The interpolated surface plot from the intensity measurement at 800 μm gives a full width at half maximum (FWHM) spot size of 5.8 μm.
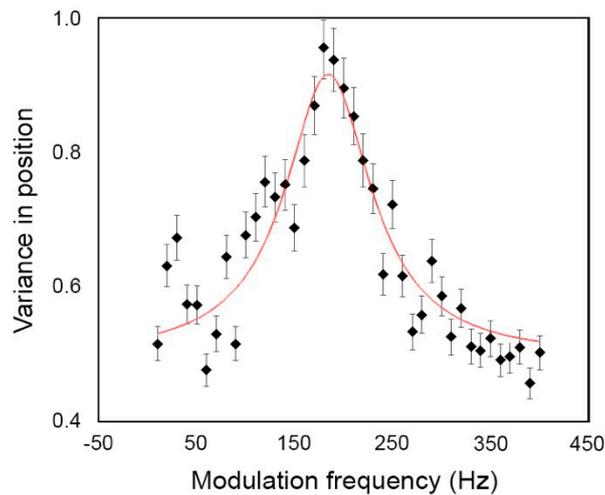

Figure 5. (**a**) The calculated intensity profile of the focal spot of the metalens calculated by Lumerical FDTD simulation and (**b**) its vertical cut of the beam through x-z plane with an FWHM of 5.4 μm.

Figure 6. A video sequence recorded during trapping of a PS bead: (**a**,**b**) bead flowed up due to heat convection of laser spot (**c**) bead entered into the trap and (**d**,**e**) remained in the trap while others on the background kept flowing up. Arrow indicates the bead of interest flowing in an upward direction.

We further explored the trapping strength of the laser beam through the metalens by modulation of the laser frequency. The technique reported [25,29] resembled the phenomenon of parametric resonance in a harmonic oscillator. The measured variance position of the bead in the trap as a function

of modulation frequency is plotted in Figure 7 without scaling since the main focus is on relative changes of the value only. The Lorentian fit of the data yields a center frequency of 180.98 ± 0.02 Hz. The trap stiffness of optical tweezers at 30 mW power is calculated from $k_{trap} = 4\pi^2 f_{trap}{}^2 m$, where m is bead mass of 5×10^{-14} kg, giving the trapping strength $k_{trap} = 6.46 \times 10^{-2}$ µN/m. With the micron-sized beads used in the experiment, the trapping force of this setup was in the order of fraction of a piconewton. The resultant force is small because metalens loses much efficiency due to low emission from nanoantennas. However, in a recent development, improved efficiency metalenses have been reported [22,30].
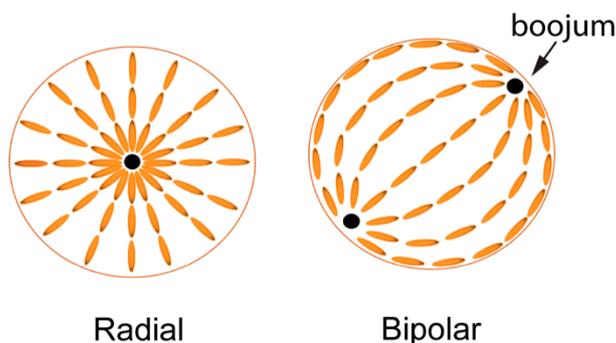

Figure 7. The variance measurement of the bead position as a function of laser modulation frequency.
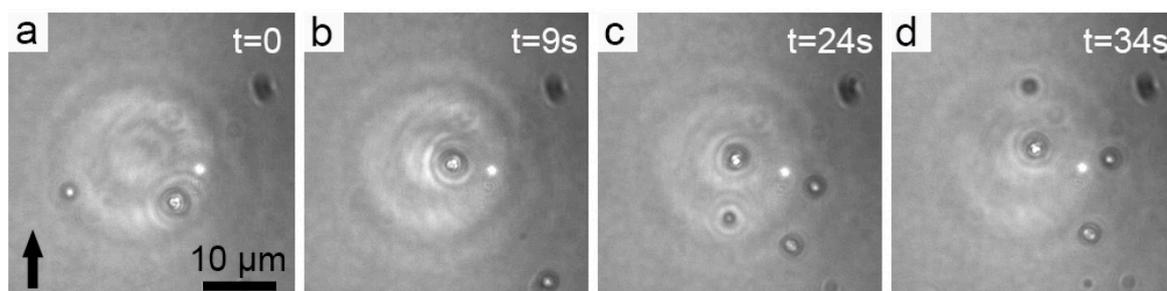
To fully employ the circularly polarized focus of the metalens, we then further applied this miniaturized metalens based laser tweezers system on birefringent NLC droplets. NLC droplets is one form of LC confinement in constricted geometries which have drawn attention from scientists for various aspects of interest. Confinements of liquid crystal directors generates various structure with different types of topological defects restricted inside due to anchoring effect at the surface [31,32]. In various technological applications, confinement of liquid crystals in the form of droplets have been employed for electro-optics purpose to control light, for example, polymer dispersed liquid crystals in smart windows or light shutters, microlasers based on liquid crystal droplets potentially applied as a bio/chemical sensing applications in aqueous environment [33,34]. The NLC droplets have also been used considerably to demonstrate the transfer of angular momentum of light in the form of rotation torque on the droplets [27,28,35–37]. Observation of defects confined inside the droplets allowed interpretation of the mechanism of angular momentum transfer from light to the droplets. Other than being rotated by light, the NLC droplets can also be switched by the electrodes [38]; these properties draw much interest as they hold promising potential applications as optical switches or rotors.

NLC droplets suspended in water were filled into the sample chamber. The droplets with radial configuration captured +1 topological defect in the middle while bipolar droplets expelled +1 defect to their surface as illustrated in Figure 8. With our metalens, we observed that trapping of NLC droplets can easily be performed as shown in a video sequence in Figure 9. With the closer observation of the droplet texture under crossed polarizers, we found radial droplets with crossed brushes in the middle and bipolar droplets possessing two boojums on the edge. These two types of droplets behaved differently under the LCP optical trap. Figure 10 shows an image sequence of the radial droplet in the optical trap. The droplet was shaken while in the optical trap with no change observed in the crossed brush texture which is typical for a symmetric configuration under rotation. Thus, with radial droplets, it is difficult to determine whether droplet rotates or not. Observation of radial droplet rotation can usually be determined from transformation of regular crossed brushes to chiral
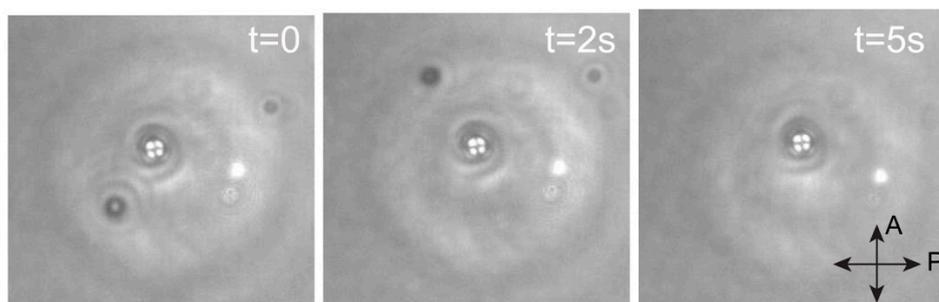
crossed brushes under higher power optical trap [27,35]. With our metalens based optical tweezers, by increasing the laser power to certain level, the metalens can suffer some damage on pattern of gold nanorods. The observation of bipolar droplets, however, is much easier to determine as the rotation can be observed from the boojum position.

Figure 8. Configurations of radial and bipolar droplets. In the radial droplet, molecules lie perpendicular to the droplet surface trapping a +1 or hedgehog defect in the middle while in the bipolar droplet, molecules lie parallel to the surface confining two boojums at the surface.
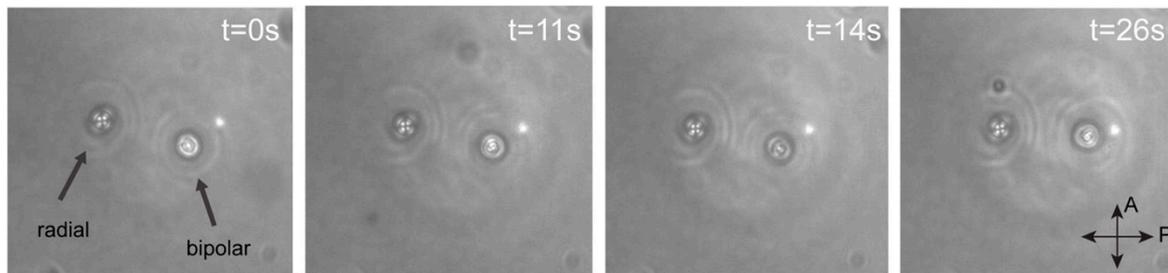

Figure 9. A video sequence showing (**a**,**b**) an NLC droplet moving upward due to heat convection and was trapped by metalens based laser tweezers. (**c**,**d**) The trapped droplet remained in the laser focus while others in the background kept flowing upward.

Figure 10. An image sequence of the radial droplet trapped by the optical tweezer. Crossed brushes represent +1 defect confined in the middle of the droplet.

Figure 11 shows both radial and bipolar droplets trapped in the laser spot. The bipolar droplet shows clear rotation in the optical trap with the texture changing all the time. With 30 mW laser tweezers, the rotation appeared to be confined in the observation plane. However, by reducing the laser power, the boojums appeared to rotate into the top view and in irregular manner since the force from circularly polarized laser trap no longer dominates. The irregular rotation was influenced by both radiation pressure of the laser and heat convection. The rotation of birefringent droplets is a strong evidence that the optical trap possesses strong enough angular momentum of light from radiation of each nanostructure acting like a local half waveplate and introducing an orientation-dependent phase

to light. This is the next step of success from the first report of metalens based optical trap [20] by adding the state of polarization of light into the optical trap.

Figure 11. Both radial and bipolar droplets were trapped by the optical tweezers. Radial droplet texture remains the same due to its symmetric configuration while bipolar droplet showed continuous rotation in the laser trap.

4. Conclusions

In summary, we have demonstrated an optical rotation of microdroplets using metalens based polarized optical tweezers on birefringent objects. Ultrathin metalenses are ideal for lab-on-a-chip systems and have a high potential to replace conventional lenses in the near future. Liquid crystal integrated well into this miniaturized optical tweezer device creating an ideal optical motor which can easily be applied into several microscopic systems for motion and flow control.

References

1. Edwards, B.; Alù, A.; Silveirinha, M.G.; Engheta, N. Experimental verification of plasmonic cloaking at microwave frequencies with metamaterials. *Phys. Rev. Lett.* **2009**, *103*, 153901. [CrossRef] [PubMed]
2. Shelby, R.A.; Smith, D.R.; Schultz, S. Experimental verification of a negative index of refraction. *Science* **2001**, *292*, 77. [CrossRef] [PubMed]
3. Valentine, J.; Zhang, S.; Zentgraf, T.; Ulin-Avila, E.; Genov, D.A.; Bartal, G.; Zhang, X. Three-dimensional optical metamaterial with a negative refractive index. *Nature* **2008**, *455*, 376. [CrossRef] [PubMed]
4. Dolling, G.; Wegener, M.; Soukoulis, C.M.; Linden, S. Negative-index metamaterial at 780 nm wavelength. *Opt. Lett.* **2007**, *32*, 53–55. [CrossRef]
5. Chen, X.; Huang, L.; Mühlenbernd, H.; Li, G.; Bai, B.; Tan, Q.; Jin, G.; Qiu, C.-W.; Zentgraf, T.; Zhang, S. Reversible Three-dimensional focusing of visible light with ultrathin plasmonic flat lens. *Adv. Opt. Mater.* **2013**, *1*, 517–521. [CrossRef]
6. Chen, X.; Huang, L.; Muhlenbernd, H.; Li, G.; Bai, B.; Tan, Q.; Jin, G.; Qiu, C.-W.; Zhang, S.; Zentgraf, T. Dual-polarity plasmonic metalens for visible light. *Nat. Commun.* **2012**, *3*, 1198. [CrossRef] [PubMed]
7. Li, J.; Mueller, J.P.B.; Wang, Q.; Yuan, G.; Antoniou, N.; Yuan, X.-C.; Capasso, F. Polarization-controlled tunable directional coupling of surface plasmon polaritons. *Science* **2013**, *340*, 331–334.
8. Yu, N.; Genevet, P.; Kats, M.A.; Aieta, F.; Tetienne, J.-P.; Capasso, F.; Gaburro, Z. Light propagation with phase discontinuities: Generalized laws of reflection and refraction. *Science* **2011**, *334*, 333–337. [CrossRef]

9.　Genevet, P.; Capasso, F.; Aieta, F.; Khorasaninejad, M.; Devlin, R. Recent advances in planar optics: From plasmonic to dielectric metasurfaces. *Optica* **2017**, *4*, 139–152. [CrossRef]

10.　Yu, N.; Aieta, F.; Genevet, P.; Kats, M.A.; Gaburro, Z.; Capasso, F. A broadband, background-free quarter-wave plate based on plasmonic metasurfaces. *Nano Lett.* **2012**, *12*, 6328–6333. [CrossRef]

11.　D'Aguanno, G.; Mattiucci, N.; Bloemer, M.; Desyatnikov, A. Optical vortices during a superresolution process in a metamaterial. *Phys. Rev. A* **2008**, *77*, 043825. [CrossRef]

12.　Yin, X.; Ye, Z.; Rho, J.; Wang, Y.; Zhang, X. Photonic spin hall effect at metasurfaces. *Science* **2013**, *339*, 1405–1407. [CrossRef] [PubMed]

13.　Shitrit, N.; Yulevich, I.; Maguid, E.; Ozeri, D.; Veksler, D.; Kleiner, V.; Hasman, E. Spin-optical metamaterial route to spin-controlled photonics. *Science* **2013**, *340*, 724–726. [CrossRef] [PubMed]

14.　Pors, A.; Nielsen, M.G.; Bernardin, T.; Weeber, J.-C.; Bozhevolnyi, S.I. Efficient unidirectional polarization-controlled excitation of surface plasmon polaritons. *Light Sci. Appl.* **2014**, *3*, e197. [CrossRef]

15.　Huang, L.; Chen, X.; Bai, B.; Tan, Q.; Jin, G.; Zentgraf, T.; Zhang, S. Helicity dependent directional surface plasmon polariton excitation using a metasurface with interfacial phase discontinuity. *Light Sci. Appl.* **2013**, *2*, e70. [CrossRef]

16.　Khorasaninejad, M.; Chen, W.T.; Devlin, R.C.; Oh, J.; Zhu, A.Y.; Capasso, F. Metalenses at visible wavelengths: Diffraction-limited focusing and subwavelength resolution imaging. *Science* **2016**, *352*, 1190–1194. [CrossRef] [PubMed]

17.　She, A.; Zhang, S.; Shian, S.; Clarke, D.R.; Capasso, F. Large area metalenses: Design, characterization, and mass manufacturing. *Opt. Express* **2018**, *26*, 1573–1585. [CrossRef] [PubMed]

18.　Ashkin, A.; Dziedzic, J.M.; Yamane, T. Optical trapping and manipulation of single cells using infrared laser beams. *Nature* **1987**, *330*, 769–771. [CrossRef] [PubMed]

19.　Friese, M.E.J.; Nieminen, T.A.; Heckenberg, N.R.; Rubinsztein-Dunlop, H. Optical alignment and spinning of laser-trapped microscopic particles. *Nature* **1998**, *394*, 348–350. [CrossRef]

20.　Tkachenko, G.; Stellinga, D.; Ruskuc, A.; Chen, M.; Dholakia, K.; Krauss, T.F. Optical trapping with planar silicon metalenses. *Opt. Lett.* **2018**, *43*, 3224. [CrossRef]

21.　Huang, L.; Chen, X.; Mühlenbernd, H.; Li, G.; Bai, B.; Tan, Q.; Jin, G.; Zentgraf, T.; Zhang, S. Dispersionless phase discontinuities for controlling light propagation. *Nano Lett.* **2012**, *12*, 5750–5755. [CrossRef] [PubMed]

22.　Chen, J.; Zhang, F.; Li, Q.; Wu, J.; Wu, L. A high-efficiency dual-wavelength achromatic metalens based on Pancharatnam-Berry phase manipulation. *Opt. Express* **2018**, *26*, 34919–34927. [CrossRef] [PubMed]

23.　Walter, F.; Li, G.; Meier, C.; Zhang, S.; Zentgraf, T. Ultrathin nonlinear metasurface for optical image encoding. *Nano Lett.* **2017**, *17*, 3171–3175. [CrossRef] [PubMed]

24.　Harada, Y.; Asakura, T. Radiation forces on a dielectric sphere in the Rayleigh scattering regime. *Opt. Commun.* **1996**, *124*, 529–541.

25.　Joykutty, J.; Mathur, V.; Venkataraman, V.; Natarajan, V. Direct measurement of the oscillation frequency in an optical-tweezers trap by parametric excitation. *Phys. Rev. Lett.* **2005**, *95*, 193902. [CrossRef] [PubMed]

26.　Grier, D.G. A revolution in optical manipulation. *Nature* **2003**, *424*, 810–816. [CrossRef]

27.　Murazawa, N.; Juodkazis, S.; Misawa, H. Characterization of bipolar and radial nematic liquid crystal droplets using laser-tweezers. *J. Phys. D Appl. Phys.* **2005**, *38*, 2923–2927. [CrossRef]

28.　Phanphak, S.; Pattanaporkratana, A.; Limtrakul, J.; Chattham, N. Precession mechanism of nematic liquid crystal droplets under low power optical tweezers. *Ferroelectrics* **2014**, *468*, 114–122. [CrossRef]

29.　Allersma, M.W.; Gittes, F.; deCastro, M.J.; Stewart, R.J.; Schmidt, C.F. Two-dimensional tracking of ncd motility by back focal plane interferometry. *Biophys. J.* **1998**, *74*, 1074–1085. [CrossRef]

30.　Byrnes, S.J.; Lenef, A.; Aieta, F.; Capasso, F. Designing large, high-efficiency, high-numerical-aperture, transmissive meta-lenses for visible light. *Opt. Express* **2016**, *24*, 5110–5124. [CrossRef]

31.　Lagerwall, J.P.F.; Scalia, G. A new era for liquid crystal research: Applications of liquid crystals in soft matter nano-, bio- and microtechnology. *Curr. Appl. Phys.* **2012**, *12*, 1387–1412. [CrossRef]

32.　Lavrentovich, O.D. Topological defects in dispersed words and worlds around liquid crystals, or liquid crystal drops. *Liq. Cryst.* **1998**, *24*, 117–126. [CrossRef]

33.　Doane, J.W.; Golemme, A.; West, J.L.; Whitehead, J.B.; Wu, B.G. Polymer dispersed liquid crystals for display application. *Mol. Cryst. Liq. Cryst.* **1988**, *165*, 511–532. [CrossRef]

34. Che, K.-J.; Yang, Y.-J.; Lin, Y.-L.; Shan, Y.-W.; Ge, Y.-H.; Li, S.-S.; Chen, L.-J.; Yang, C.J. Microfluidic generation of cholesteric liquid crystal droplets with an integrative cavity for dual-gain and controllable lasing. *Lab Chip* **2019**, *19*, 3116–3122. [CrossRef] [PubMed]

35. Brasselet, E.; Murazawa, N.; Misawa, H.; Juodkazis, S. Optical vortices from liquid crystal droplets. *Phys. Rev. Lett.* **2009**, *103*, 103903. [CrossRef] [PubMed]

36. Juodkazis, S.; Matsuo, S.; Murazawa, N.; Hasegawa, I.; Misawa, H. High-efficiency optical transfer of torque to a nematic liquid crystal droplet. *Appl. Phys. Lett.* **2003**, *82*, 4657–4659. [CrossRef]

37. Wood, T.A.; Gleeson, H.F.; Dickinson, M.R.; Wright, A.J. Mechanisms of optical angular momentum transfer to nematic liquid crystalline droplets. *Appl. Phys. Lett.* **2004**, *84*, 4292–4294. [CrossRef]

38. Cairns, D.R.; Sibulkin, M.; Crawford, G.P. Switching dynamics of suspended mesogenic polymer microspheres. *Appl. Phys. Lett.* **2001**, *78*, 2643–2645. [CrossRef]